LETTER

doi:10.1038/nature13796

Direct observations of evolving subglacial drainage beneath the Greenland Ice Sheet

Lauren C. Andrews[1,2], Ginny A. Catania[1,2], Matthew J. Hoffman[3,4], Jason D. Gulley[1,5], Martin P. Lüthi[6,7], Claudia Ryser[7], Robert L. Hawley[8] & Thomas A. Neumann[4]

Seasonal acceleration of the Greenland Ice Sheet is influenced by the dynamic response of the subglacial hydrologic system to variability in meltwater delivery to the bed[1,2] via crevasses and moulins (vertical conduits connecting supraglacial water to the bed of the ice sheet). As the melt season progresses, the subglacial hydrologic system drains supraglacial meltwater more efficiently[1–4], decreasing basal water pressure[4] and moderating the ice velocity response to surface melting[1,2]. However, limited direct observations of subglacial water pressure[4–7] mean that the spatiotemporal evolution of the subglacial hydrologic system remains poorly understood. Here we show that ice velocity is well correlated with moulin hydraulic head but is out of phase with that of nearby (0.3–2 kilometres away) boreholes, indicating that moulins connect to an efficient, channelized component of the subglacial hydrologic system, which exerts the primary control on diurnal and multi-day changes in ice velocity. Our simultaneous measurements of moulin and borehole hydraulic head and ice velocity in the Paakitsoq region of western Greenland show that decreasing trends in ice velocity during the latter part of the melt season cannot be explained by changes in the ability of moulin-connected channels to convey supraglacial melt. Instead, these observations suggest that decreasing late-season ice velocity may be caused by changes in connectivity in unchannelized regions of the subglacial hydrologic system. Understanding this spatiotemporal variability in subglacial pressures is increasingly important because melt-season dynamics affect ice velocity beyond the conclusion of the melt season[8–10].

In the ablation zone of the Greenland Ice Sheet (GIS), moulins deliver surface melt to the base of the ice sheet[11], where fluctuations in meltwater supply modulate ice motion[2,12,13]. The relationship between surface melting and ice velocity is thought to reflect the structure and evolution of the subglacial hydrologic system[1,2,12,13]. Ice acceleration occurs when meltwater input exceeds the hydraulic capacity of the subglacial system, causing englacial and subglacial water storage and resulting in the widespread reduction in basal friction[12–14]. Subglacial water pressure and ice velocity of the GIS are thought to remain elevated until a channelized drainage system develops, decreasing subglacial water pressure and ice velocity by efficiently routeing surface meltwater to the glacier terminus via moulins[1,3,4]. Short-term increases in ice velocity can persist following channelization owing to temporary imbalances between the capacity of this efficient drainage system and the magnitude of surface water input[14,15] from melt[12] and precipitation events[10] or supraglacial lake drainage[13,16]. In this paradigm, channelized systems have been considered the key component governing ice-velocity sensitivity to supraglacial water input. Accordingly, moulin hydraulic head and ice velocity should both decrease seasonally as drainage efficiency increases.

Despite observations of decreasing minimum velocities during much of the melt season[1,9,10,13], the role of channelization beneath some regions of the GIS may be limited by shallow surface slopes and limited basal conduit meltback[6]. An extensive body of research on alpine glaciers highlights the central role of channelization in subglacial drainage evolution[14,17–19], but also documents significant complexity in the unchannelized regions of the bed[17–22]. Borehole observations reveal that some portions of the unchannelized region transmit meltwater that is sourced from channels[17,18], whereas other unchannelized regions of the bed are hydraulically isolated and receive little to no direct water input[17,21,22]. Basal pressure in these isolated regions responds to changes in the active drainage regions through transfer of mechanical support[8,17,22] or as cavity volumes[21] or pore volumes in subglacial sediment fluctuate in response to ice motion. While changing connectivity between active and isolated components of the subglacial drainage system has been directly observed[17,22], it is not believed to drive seasonal trends in ice velocity on alpine glaciers owing to the dominant control of subglacial channels[17,18,21].

Here we use borehole hydraulic heads to explore the response of the unchannelized region of the bed to channelized regions. Few direct measurements of water pressure have been made in channelized regions of the GIS bed[4,6], owing to the limited number of borehole studies[5–7] and their inherently limited spatial extent. Consequently, we also measure water level in three different moulins to constrain hydraulic head in active regions of the subglacial hydrologic system. These borehole and moulin hydraulic heads are coupled with coincident measurements of surface ice velocity, bed separation, and air temperature to characterize relationships between ice dynamics and the subglacial hydrologic system during the 2011 and 2012 melt seasons.

At our primary field site in the ablation zone of Sermeq Avannarleq in western Greenland (Fig. 1; 69° 27′ N, 49° 53′ W; Extended Data Table 1), we drilled seven boreholes to the bed using a hot water drill and instrumented three of these with pressure transducers in 2011 (ref. 7) (Methods). The ice thickness in our instrumented boreholes was between 614 m and 624 m, and each borehole either drained slowly or did not drain before closure. The combination of gradual drainage following drilling and results from pump tests suggest borehole connection to unchannelized regions of the bed[17,18,22] (Methods). During 2011, we instrumented the FOXX moulin, about 0.3 km southwest of the boreholes, with a pressure transducer. In 2012, we instrumented moulins 3 and 4 with pressure transducers, 1.6 km and 1.9 km from the boreholes, respectively (Methods). Because moulin instrumentation could not proceed until the snowline had retreated past the field sites, these moulin measurements capture relationships between subglacial hydrology and ice motion after channelization is inferred to have begun[4]. We derive ice velocity and bed separation from Global Positioning System (GPS) installations at several locations (Methods; Extended Data Fig. 2). We use meteorological observations from a weather station co-located with the FOXX GPS to determine periods of increasing surface melt (Methods).

The magnitude and phase of moulin and borehole measurements differ substantially in their relationship to ice velocity (Fig. 2; Extended Data Fig. 1), suggesting that each monitored a different component of the subglacial system. Moulin hydraulic heads were highly variable, with

[1]Institute for Geophysics, Jackson School of Geosciences, The University of Texas at Austin, Austin, Texas 78758, USA. [2]Department of Geological Sciences, Jackson School of Geosciences, The University of Texas at Austin, Austin, Texas 78712, USA. [3]Fluid Dynamics and Solid Mechanics Group, Los Alamos National Laboratory, Los Alamos, New Mexico 87545, USA. [4]NASA Goddard Space Flight Center, Greenbelt, Maryland 20771, USA. [5]Department of Geological and Mining Engineering and Sciences, Michigan Technological University, Houghton, Michigan 49931, USA. [6]Glaciology and Geomorphodynamics Group, Physical Geography Division, Department of Geography, University of Zürich, 8057 Zürich, Switzerland. [7]Laboratory of Hydraulics, Hydrology and Glaciology, Swiss Federal Institute of Technology (ETH) Zürich, 8093 Zürich, Switzerland. [8]Department of Earth Sciences, Dartmouth College, Hanover, New Hampshire 03755, USA.

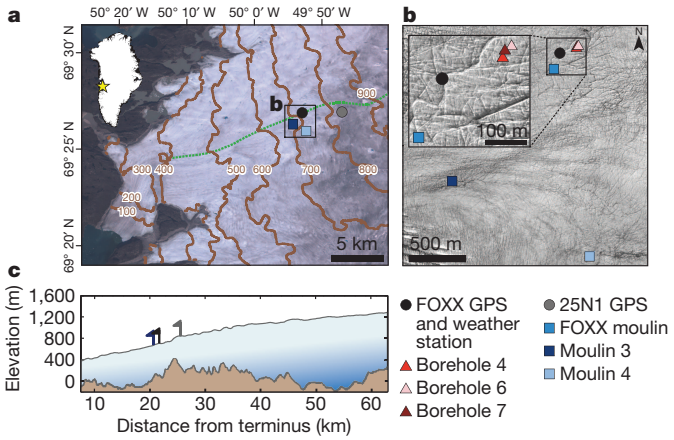

Figure 1 | Study area in the ablation zone of the western Greenland Ice Sheet. a, Landsat-7 image of Sermeq Avannarleq. Ice-surface contours (marked in metres; brown) are derived from the Greenland Ice Mapping Project (GIMP) surface DEM[29]. Site symbols are indicated in the key. The black box indicates the area in **b**. A 2012 Center for Remote Sensing of Ice Sheets (CReSIS) flight line[30] (green) provides the cross-section in **c**. **b**, 2009 Worldview-2 image of the study area with site locations indicated. **c**, Bed and surface elevations from radar depth sounding[30]. Moulin 3 (navy), FOXX (black) and 25N1 (grey) are projected onto the flight line. Moulin 4 projects onto the FOXX location.

a mean diurnal fluctuation of approximately 95 ± 47 m (about 17% of overburden) during 2012 and minimum values (about 70% of overburden) well below the ice surface. In addition, hydraulic heads in moulins 3 and 4 are synchronous, despite being located in different supraglacial drainage basins and 1.5 km apart (Extended Data Table 2). This similarity in hydraulic heads suggests pressure equalization within an efficient system[23] that connects these moulins at the bed[3,4]. Further, numerical analysis supports the existence of subglacial channels in our study area (Methods; Extended Data Fig. 3). During periods of steady supraglacial input channel development via meltback may be limited; however, observed melt-event perturbations temporarily increase channel volume, allowing greater transmission of water. From these observations, we infer that moulin hydraulic head reflects subglacial water pressure within a moulin-connected channel system[4,17,18], which appears to increase in efficiency only over short timescales.

In contrast, our boreholes display high mean hydraulic head (close to or above overburden) and low-amplitude diurnal variability (less than 25 m or <5% of overburden). Borehole hydraulic heads are anti-correlated with ice velocity (Fig. 3a, b; Extended Data Table 2). These systematic differences between moulins and boreholes further suggest that moulins connect to a channelized component of the drainage system, while boreholes monitor an isolated region of the bed unconnected to the channelized system[17,18,21,22] (Methods).

Strong correlations between diurnal peaks in moulin hydraulic heads and ice velocity suggest that pressure variability in the channelized drainage system reduces basal friction in an adjacent active but unchannelized component of the hydraulic system and drives diurnal ice acceleration, as observed in alpine glaciers[14]. However, on longer timescales the relationship between moulin hydraulic head and ice velocity is characterized by hysteresis. In both 2011 and 2012, ice velocity decreases as the melt season progresses, despite relatively constant moulin hydraulic heads (Fig. 3c; Extended Data Fig. 4). Further, neither the minimum nor maximum daily moulin head decreases over the observation period, as would be expected with increasing efficiency, suggesting that pressure decreases in the efficient, channelized system do not control decreases in ice velocity during the latter portion of the melt season (Fig. 3d). Therefore, while variability in moulin head appears to drive diurnal and multi-day velocity

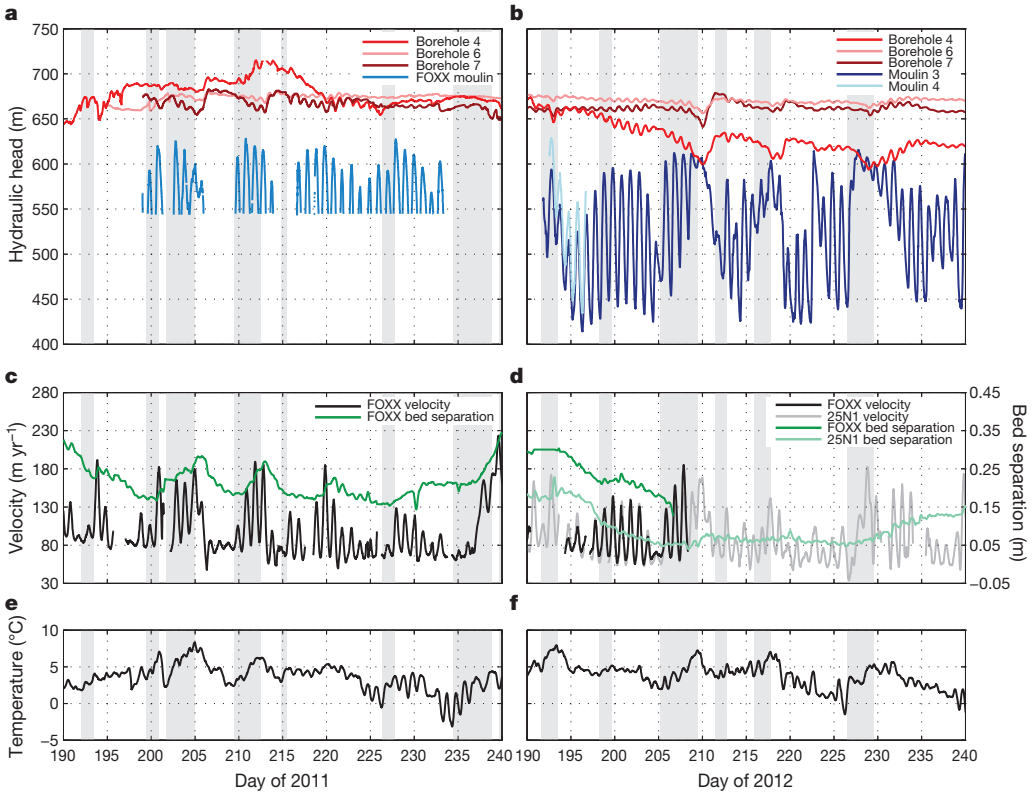

Figure 2 | Borehole and moulin hydraulic head and ice-surface velocity during 2011 and 2012. a, 2011 hydraulic head measurements from the FOXX moulin (blue), borehole 4 (red), borehole 6 (pink) and borehole 7 (dark red). **b**, 2012 data from moulin 3 (navy) and moulin 4 (light blue). Borehole colours are as in 2011 (**a**). **c**, 2011 GPS-derived ice velocity (black) and bed separation (green) for FOXX. **d**, 2012 GPS-derived ice velocity for FOXX and 25N1 (grey) and bed separation for FOXX and 25N1 (light green). **e**, **f**, 6-h averaged 2-m air temperature for 2011 and 2012. Grey bars in all panels indicate periods identified as melt events.

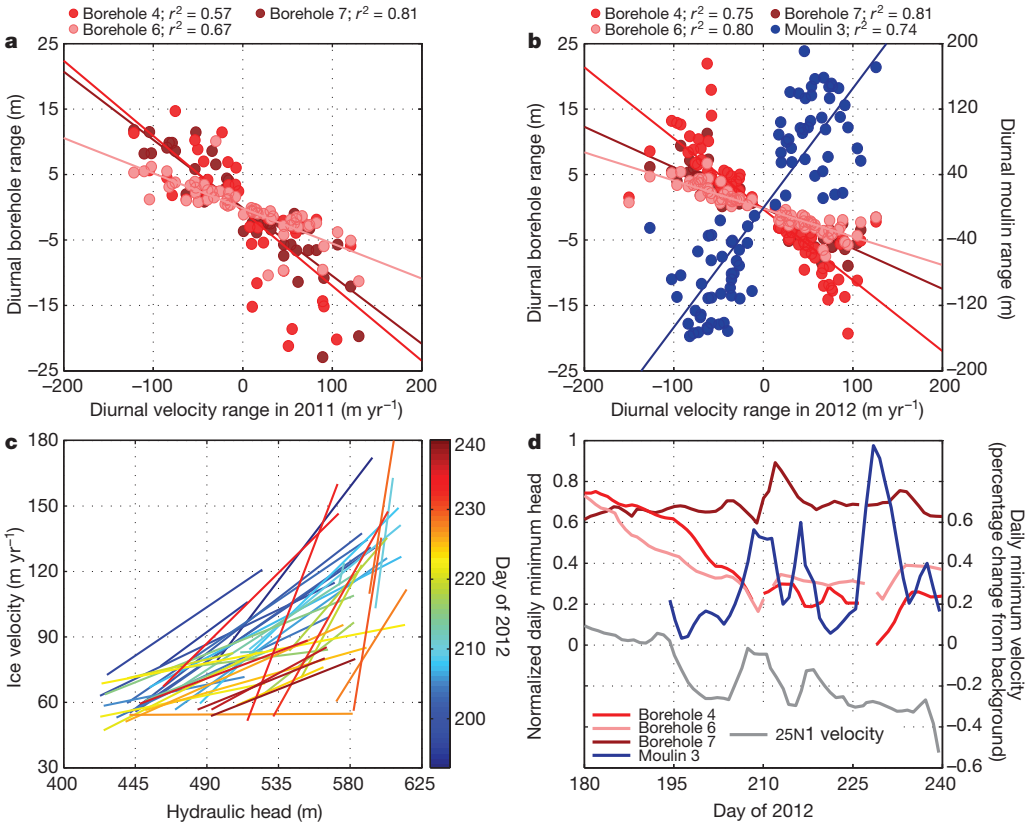

Figure 3 | Relationships between hydraulic head and ice-surface velocity. **a**, Linear regression between the magnitude of diurnal changes in ice velocity and borehole and moulin hydraulic head for 2011 ($p < 0.05$; borehole 4 $n = 48$, borehole 6 $n = 59$, borehole 7 $n = 50$). **b**, Linear regression between the magnitude of diurnal changes in ice velocity and borehole and moulin hydraulic head between days 192 and 240 in 2012 ($p < 0.05$; borehole 4 $n = 80$, borehole 6 $n = 79$, borehole 7 $n = 75$, moulin 3 $n = 85$). Days when borehole hydraulic head and ice velocity are in phase are excluded. **c**, Daily maximum and minimum moulin hydraulic head plotted against associated ice velocity for 2012. **d**, Normalized daily minimum hydraulic heads and ice velocity as a percentage of winter background for 2012. The minimum values are smoothed over 5 days.

variations, longer-term decreases in ice velocity are potentially due to decreasing water pressure in the unchannelized regions of the subglacial hydrologic system.

As observed in alpine glaciers, isolated components of the subglacial hydrologic system may act to resist ice acceleration[21]. Previous studies demonstrate that high (above overburden) water pressures out of phase with ice velocity may be caused by transfer of mechanical support from channelized regions of the bed to isolated regions[7,17,19,22]. However, the diurnal range of borehole hydraulic heads is more strongly anti-correlated with the diurnal range of ice velocity than with the diurnal range of water pressure in nearby active regions of the bed (Methods), suggesting that borehole hydraulic head variability is at least partly the result of non-locally generated sliding[21]. In this proposed mechanism, pressurization of neighbouring regions of the bed that have an efficient connection to the channelized system induces sliding, which is transmitted to these unconnected areas by stress transfer laterally within the ice. In turn, water pressure in unconnected regions of the bed decreases as the volume of bedrock cavities increases through sliding[21] or as basal sediments deform[24,25] without a commensurate water influx. A combination of these processes results in a dynamic water pressure environment, despite the apparent hydraulic isolation of these regions of the bed.

Negative feedback between increased ice velocity and decreased water pressure in unconnected regions can act to limit sliding[20,21] and potentially control minimum ice velocity. This resistance to sliding probably varies both spatially and temporally, owing to changes in connectivity within the isolated system[17,22]. Although borehole hydraulic heads are typically anti-correlated with ice velocity, some boreholes experienced infrequent periods when pressures are in phase with ice velocity following large melt events (for example, on days 211–218 of 2011 in borehole 6, Fig. 2a). These in-phase periods may indicate ephemeral connections to the unchannelized but interconnected parts of the drainage system, which occur when the hydraulic capacity of the subglacial drainage system is overwhelmed and water flows out of conduits into the surrounding unchannelized system[4,12,14,26].

While long-term decreases in ice velocity have previously been attributed to decreasing subglacial water pressure caused by increased channelization[1,9,10], our results suggest that during the latter part of the melt season, the spatial extent of the unchannelized system is a primary control on ice velocity. Basal traction is a function of both the interconnected and isolated regions of the unchannelized system[21]. Therefore, increasing the spatial extent of the interconnected system, at the expense of the isolated system, should result in a larger fraction of the bed at lower water pressures. Gradually increasing the connectivity of the isolated system (that is, opening or enlargement of flow pathways) would have a similar result.

These processes could increase basal traction and decrease ice velocity without a change in the efficiency of the channelized system[21]. Indeed, we observe a gradual decrease in water pressure in two of three boreholes (boreholes 4 and 6; Figs 3d; Extended Data Fig. 1), implying increasing connectivity to active regions of the bed. This process is also observed at a second field site in 2011 (Methods). These reductions in subglacial pressure match well with velocity trends (Fig. 3d), suggesting that systematically decreasing pressures within the isolated system are occurring. The observed decreases in water pressure may result in a higher spatially averaged basal traction at the end of the melt season that persists after meltwater inputs cease. Consequently, this mechanism could explain the winter mediation of summer acceleration[9,10].

Our results suggest that the subglacial drainage system consists of three components that exert varying control on ice velocity over different

spatiotemporal domains: a moulin-connected channelized system that transports the available meltwater efficiently; an active, interconnected unchannelized system strongly influenced by the channelized system; and an isolated system that responds passively to changes in bed separation because water flow is slow or absent. The spatiotemporal extents of these domains are probably highly variable, with the spatial extent of each component controlled by the spatial distribution of moulin locations[27], basal and surface topography[28] and the hydraulic conductivity of basal sediments[24,25].

Direct observations of multiple components of the subglacial hydrologic system illustrate how subglacial drainage efficiency modulates ice dynamics across multiple timescales. The degree of control that each component of the subglacial system exerts on ice velocity depends critically on the period considered. Our data from a sector of the GIS ablation zone indicate that the drainage efficiency of the channelized system does not change substantially during the latter portion of the melt season. Instead, evolving efficiency of non-channelized drainage systems can explain the observed trends in ice velocity during that time. Thus, we caution against the application of channel-only models to explore the seasonal relationship between subglacial hydrology and the ice dynamics of the GIS. Future work should consider the seasonal evolution of all observed components of the subglacial hydrologic system, including isolated regions of the bed. Such investigations are increasing in importance as new results suggest that the melt-season behaviour of the subglacial system affects ice dynamics in the ablation zone[9,10] and, potentially, farther inland[8] after the melt season.

Online Content Methods, along with any additional Extended Data display items and Source Data, are available in the online version of the paper; references unique to these sections appear only in the online paper.

Received 24 February; accepted 22 August 2014.

1. Bartholomew, I. *et al.* Seasonal evolution of subglacial drainage and acceleration in a Greenland outlet glacier. *Nature Geosci.* **3,** 408–411 (2010).
2. Sundal, A. V. *et al.* Melt-induced speed-up of Greenland ice sheet offset by efficient subglacial drainage. *Nature* **469,** 521–524 (2011).
3. Chandler, D. M. *et al.* Evolution of the subglacial drainage system beneath the Greenland Ice Sheet revealed by tracers. *Nature Geosci.* **6,** 195–198 (2013).
4. Cowton, T. *et al.* Evolution of drainage system morphology at a land-terminating Greenlandic outlet glacier. *J. Geophys. Res.* **118,** 1–13 (2013).
5. Lüthi, M., Funk, M., Iken, A., Gogineni, S. & Truffer, M. Mechanisms of fast flow in Jakobshavn Isbræ, West Greenland: Part III. Measurements of ice deformation, temperature and cross-borehole conductivity in boreholes to the bedrock. *J. Glaciol.* **48,** 369–385 (2002).
6. Meierbachtol, T., Harper, J. & Humphrey, N. Basal drainage system response to increasing surface melt on the Greenland Ice Sheet. *Science* **341,** 777–779 (2013).
7. Ryser, C. *et al.* Sustained high basal motion of the Greenland Ice Sheet revealed by borehole deformation. *J. Glaciol.* **60,** 647–660 (2014).
8. Doyle, S. *et al.* Persistent flow acceleration within the interior of the Greenland ice sheet. *Geophys. Res. Lett.* **41,** 899–905 (2014).
9. Sole, A. *et al.* Winter motion mediates dynamic response of the Greenland Ice Sheet to warmer summers. *Geophys. Res. Lett.* **40,** 3940–3944 (2013).
10. Tedstone, A. J. *et al.* Greenland Ice Sheet motion insensitive to exceptional meltwater forcing. *Proc. Natl Acad. Sci. USA* **110,** 19719–19724 (2013).
11. Catania, G. A. & Neumann, T. A. Persistent englacial drainage features in the Greenland Ice Sheet. *Geophys. Res. Lett.* **37,** L02501 (2010).
12. Bartholomew, I. *et al.* Short-term variability in Greenland Ice Sheet motion forced by time-varying meltwater drainage: implications for the relationship between subglacial drainage system behavior and ice velocity. *J. Geophys. Res.* **117,** F03002 (2012).
13. Hoffman, M. J., Catania, G. A., Neumann, T. A., Andrews, L. C. & Rumrill, J. A. Links between acceleration, melting, and supraglacial lake drainage of the western Greenland Ice Sheet. *J. Geophys. Res.* **116,** F04035 (2011).
14. Bartholomaus, T. C., Anderson, R. S. & Anderson, S. P. Response of glacier basal motion to transient water storage. *Nature Geosci.* **1,** 33–37 (2008).
15. Schoof, C. Ice-sheet acceleration driven by melt supply variability. *Nature* **468,** 803–806 (2010).
16. Das, S. B. *et al.* Fracture propagation to the base of the Greenland Ice Sheet during supraglacial lake drainage. *Science* **320,** 778–781 (2008).
17. Gordon, S. *et al.* Seasonal reorganization of subglacial drainage inferred from measurements in boreholes. *Hydrol. Processes* **12,** 105–133 (1998).
18. Hubbard, B. P., Sharp, M. J., Willis, I. C., Nielsen, M. K. & Smart, C. C. Borehole water-level variations and the structure of the subglacial hydrological system of Haut Glacier d'Arolla, Valais, Switzerland. *J. Glaciol.* **41,** 572–583 (1995).
19. Mair, D. *et al.* Hydrological controls on pattern of surface, internal and basal motion during three 'spring events': Haut Glacier d'Arolla, Switzerland. *J. Glaciol.* **49,** 555–567 (2003).
20. Hoffman, M. & Price, S. Feedbacks between coupled subglacial hydrology and glacier dynamics. *J. Geophys. Res.* **119,** 411–436 (2014).
21. Iken, A. & Truffer, M. The relationship between subglacial water pressure and velocity of Findelengletscher, Switzerland, during its advance and retreat. *J. Glaciol.* **73,** 328–338 (1997).
22. Murray, T. & Clarke, G. K. C. Black-box modeling of the subglacial water system. *J. Geophys. Res.* **100,** 10231–10245 (1995).
23. Covington, M. D. *et al.* Quantifying the effects of glacier conduit geometry and recharge on proglacial hydrograph form. *J. Hydrol.* **414–415,** 59–71 (2012).
24. Dow, C. F. *et al.* Seismic evidence of mechanically weak sediments underlying Russell Glacier, West Greenland. *Ann. Glaciol.* **54,** 135–141 (2013).
25. Walter, F., Chaput, J. & Lüthi, M. P. Thick sediments beneath Greenland's ablation zone and their potential role in future ice sheet dynamics. *Geology* **42,** 487–490 (2014).
26. Hewitt, I. J. Seasonal change in ice sheet motion due to melt water lubrication. *Earth Planet. Sci. Lett.* **371–372,** 16–25 (2013).
27. Gulley, J. D. *et al.* The effect of discrete recharge by moulins and heterogeneity in flow-path efficiency at glacier beds on subglacial hydrology. *J. Glaciol.* **58,** 926–940 (2012).
28. Joughin, I. *et al.* Influence of ice-sheet geometry and supraglacial lakes on seasonal ice-flow variability. *Cryosphere* **7,** 1185–1192 (2013).
29. Howat, I. M., Negrete, A. & Smith, B. E. The Greenland Ice Mapping Project (GIMP) land classification and surface elevation datasets. *Cryosphere* **8,** 1509–1518 (2014).
30. Gogineni, P. *CReSIS Radar Depth Sounder Data* http://data.cresis.ku.edu/ (2012).

Acknowledgements This project was supported by United States National Science Foundation grants OPP-0908156, OPP-0909454 and ANT-0424589 (to CReSIS), Swiss National Science Foundation grant 200021_127197, and National Geographic Society grant 9067-12. L.C.A. was also supported by UTIG Ewing-Worzel and Gale White Graduate Student Fellowships. M.J.H. was also supported by NASA Cryospheric Sciences and Climate Modeling Programs within the US Department of Energy, Office of Science. J.D.G. was also supported by an NSF Postdoctoral Fellowship (EAR-0946767). Logistical support was provided by CH2MHill Polar Services. The GPS base station and several on-ice GPS units were provided by the UNAVCO facility with support from the NSF and NASA under cooperative agreement EAR-0735156. The University of Minnesota Polar Geospatial Center, funded under NSF OPP collaborative agreement ANT-1043681, provided WorldView imagery. We thank K. M. Schild, J. A. MacGregor, J. D. Nowinski, B. F. Morriss and others for assistance in the field.

Author Contributions G.A.C., J.D.G., M.P.L., R.L.H. and T.A.N. designed this study. L.C.A., R.L.H., M.J.H., M.P.L., C.R. and J.D.G. performed the fieldwork. L.C.A. analysed the results and wrote the manuscript. All authors discussed the results and edited the manuscript.

Author Information Reprints and permissions information is available at www.nature.com/reprints. The authors declare no competing financial interests. Readers are welcome to comment on the online version of the paper. Correspondence and requests for materials should be addressed to L.C.A. (landrews@ig.utexas.edu).

METHODS

Seasonal data presentation. To clearly present diurnal variability in the measured parameters, the time series is shortened to the period of time over which moulin hydraulic heads are measured (Fig. 2). During 2011, velocity and bed separation were measured throughout the melt season; in 2012, all parameters except moulin pressures were recorded over the entire melt season (Extended Data Fig. 1).

Borehole drilling and instrumentation. During 2011, 13 boreholes were drilled at two sites, seven at FOXX (Fig. 1; 69° 27′ N, 49° 53′ W) and six at GULL (69° 27′ N, 49° 43′ W), using hot water drilling techniques and equipment[5,7,31,32]. Drill water had a consistent temperature and pressure of 80 °C and 8 MPa, respectively. At FOXX, three boreholes were instrumented with pressure transducers at depths between 614 m and 624 m (Extended Data Table 1). In Greenland, thick cold ice results in rapid (less than a day) closure of boreholes, eliminating the influence of surface water input. Further, the volume of the boreholes is assumed to be small relative to the subglacial system. Therefore, we assume that these boreholes function as accurate manometers of the subglacial system.

Two boreholes (boreholes 4 and 6) were instrumented with the Swiss Federal Institute of Technology (ETH) designed digital borehole sensor system (DIBOSS)[7]. Borehole 7 was instrumented with a Geokon 4500HD piezometer. All sensors were connected to the surface via cables able to accommodate an additional 20% strain before breaking (Cortland Cable). Campbell Scientific CR1000 data loggers were used for switching power supply and recording sensor measurements via CFM100 storage modules. The sampling interval ranged from 1 min to 15 min. Data were decimated to 15-min intervals for analysis in this paper. All units remained powered between summer 2011 and spring 2013.

Several observations during and following the drilling process indicate that the boreholes connected to the ice–bed interface: (1) all boreholes reached similar depths of 614 to 624 m; these depths are similar to, though slightly deeper than, depths expected from a 2012 CReSIS depth-sounding radar track through the FOXX field site[30]; (2) drilling only ceased when pressures at the drill tip rapidly decreased; (3) boreholes 4 and 6 drained slowly over the course of several hours; and (4) pump tests were performed in boreholes 4 and 6, forcing a connection to the subglacial system. Changes associated with pump tests were ephemeral and boreholes gradually reverted to their pre-pump test state. Borehole 7 also connected to the bed because, even though it did not drain before closure, the diurnal lags and melt event pressure variations in borehole 7 are similar to those observed in boreholes 4 and 6 over the course of both melt seasons.

Borehole hydraulic heads were calculated from measured borehole pressure (from installed pressure transducer), surface elevation and borehole depth:

$$h = \frac{P_w}{\rho_w g} + z_{bed} \quad (1)$$

where h is total hydraulic head. P_w is directly measured from borehole sensors, but is also equal to $\rho_w g h_w$. The density of water is ρ_w; g is the acceleration due to gravity and h_w is water height. z_{bed} is the bed elevation determined from GPS-derived ice-surface elevation and measured borehole depth. Representing borehole data as hydraulic head allows us to determine water level absolutely, as measured from sea-level in different locations.

Moulin instrumentation and measurements. Moulins were instrumented in both the 2011 (FOXX moulin) and 2012 (moulins 3 and 4) melt seasons (Extended Data Table 1). Water pressures were measured using the Geokon 4500 (2011) or 4500HD (2012) piezometers on armoured cables ranging from 400 m to 600 m in length. Campbell Scientific CR1000 data loggers were used for switching power supply and recording sensor measurements via CFM100 storage modules. Water pressures were corrected for local barometric pressure as measured at the FOXX GPS station (2011) and moulin 3 (2012). Sampling intervals were 5 min or 15 min. Data were decimated to 15 min for analysis except where noted.

Moulin instrumentation is complicated by moulin geometry and water-level fluctuations that occur during pressure sensor installation. To constrain the absolute elevation of the pressure sensor in each moulin several corrections to the measured moulin water level must be made. These corrections include adjustment for the rise of water levels during the sensor installation and the mean slope of the conduit.

During sensor installation, we periodically paused while lowering to observe the water-level rise with the sensor held in a static position. These pauses allowed us to constrain the total change in water level over the course of sensor installation. Once the water level was corrected to a static level, we corrected for the slope of the moulin. However, it is important to note that moulins in Greenland are generally nearly vertical[11], so this correction is small. We subtracted the corrected sensor depth from the GPS-derived surface elevation at each site to constrain the vertical sensor location. Sensor elevation and measured water level provide hydraulic head without the need to use poorly constrained ice thicknesses and bed elevations at moulin sites.

Owing to the possibly complex geometry of moulins, the error in sensor location is higher than the error in borehole-sensor locations. We estimate the error in absolute head measurements to be approximately 20 m. Uncertainty related to absolute head measurements does not affect measurements of relative changes, such as diurnal amplitudes of hydraulic head. The sensor in moulin 3 is near the bed of the ice sheet, as indicated by the continual increase in water as the sensor was lowered and because the total cable length deployed was similar to the local ice thickness. The sensor in moulin 4 is approximately 175 m from the bed, on the basis of similar observations. The 2011 sensor in the FOXX moulin is much shallower, as indicated by the truncated pressure record. Owing to the deployment techniques, the absolute sensor location is not as well constrained in 2011 as in 2012. We estimate the FOXX sensor location to be 455 m above the bed.

Moulins connect directly to highly efficient components of the subglacial system[27] and have previously been used with varying levels of success to measure the water level of the channelized component of the subglacial system[4,33–35]. Although moulins are not considered manometers, measured moulin pressures can be considered equivalent to subglacial water pressures within the channelized system, because pressure changes in multiple moulins are coincident (Extended Data Table 2), despite drainage basins of differing sizes and discharges. The volume of water in a moulin is large relative to the volume of water being discharged at the bed, so water flow within the moulin is slow[36]; we therefore neglect the velocity head.

In addition, to be considered effective measures of water pressure, the volume of water within the moulin must be small when compared to the volume of water in the channelized system. Considering that large portions of the channelized system are connected[3,4], the total volume in a single moulin is probably small relative to the total water volume within the channelized system. With these assumptions, we consider the measured moulin pressures to be representative of subglacial pressures in the efficient component of the subglacial system.

Coincident observations. Over the course of 4 days (approximately day 192.5 to day 196.5), we were able to monitor the water level in two moulins concurrently (Fig. 2b). These observations suggest that the hydraulic heads of both moulins behave very similarly, with peaks, and even small perturbations, occurring in both moulins at the same time (Extended Data Table 2). We did not calculate the hydraulic gradient between the two moulins because the length of the subglacial channel is unknown and channel paths may diverge from those predicted by hydraulic potential theory[27]. However, we do use the head difference as a proxy for the hydraulic gradient[17], assuming that the subglacial channel does not alter its path significantly over the course of the melt season.

Ice velocity and bed separation. Kinematic GPS positions were determined using carrier-phase differential processing relative to a bedrock mounted reference station using Track 1.24[37] and techniques described by ref. 13. GPS observations at all stations were logged at 15-s intervals, and the relative position of each on-ice station was determined at this frequency. Each 15-s time series was smoothed with a 6-hour moving average, applied to reduce spurious signals associated with GPS uncertainties, and then decimated to 15-min time series. Using the mean error generated during processing, the horizontal and vertical position errors for 2011 (and 2012) were ±9.9 cm (±8.8 cm) and ±1 cm (±1 cm) respectively, with a velocity uncertainty of ~8.8 m yr^{-1} (~7.7 m yr^{-1}).

During 2012, the antenna pole for the FOXX GPS station melted out owing to higher than expected ablation rates. The data become unreliable after day 208, and the station ceased recording by day 215. Owing to the similarity between FOXX and 25N1 data (Fig. 2; Extended Data Fig. 1), the 25N1 GPS data were used for analysis of 2012 data. Over the entire melt season, ice velocities at both stations display the characteristic decrease in daily minima[13] (Extended Data Fig. 1).

Bed-separation calculations were performed incorporating additional observations from nearby GPS stations and following the procedures described in detail in previous work[13]. Both longitudinal (along flow) and lateral (across flow) strain rates $\dot{\varepsilon}$ were calculated from GPS data as follows:

$$\dot{\varepsilon} = \frac{1}{l_0}\frac{\Delta l}{\Delta t} \quad (2)$$

where Δl is the change in baseline distance between stations, Δt is the change in time between measurements and l_0 is the initial baseline distance. Longitudinal strain at our field location is generally compressional over the course of the season. During 2012, GPS malfunction prevented the collection of data from 19N1 and decreased the availability of data from the FOXX GPS; bed separation was therefore calculated between 25N1 and GULL and is presented as a proxy (Fig. 2 and Extended Data Fig. 1). During 2012, malfunction of a GPS station used to determine lateral strain between 25N1 and GULL required that we assume a constant lateral strain for bed separation calculations after day 205.

We approximate the vertical strain rate $\dot{\varepsilon}$ with the continuity equation, assuming ice is incompressible:

$$\dot{\varepsilon}_{zz} = -(\dot{\varepsilon}_{xx} + \dot{\varepsilon}_{yy}) \quad (3)$$

where x, y and z represent the longitudinal, lateral and vertical directions, respectively.

Following accepted methodology[38–43], we decompose the vertical motion measured by the GPS as:

$$w_s = u_b \tan(\alpha) + \dot{\varepsilon}_{zz} H + \dot{c} \quad (4)$$

where u is the horizontal velocity, α is the bed slope, H is the ice thickness at the GPS station, as measured by borehole depth, and $\dot{c}$ is the rate of bed separation (cavity opening and/or till dilation). Subscripts 's' and 'b' refer to the surface and bed of the ice sheet, respectively. Equation (4) is solved for $\dot{c}$ using observations of the other parameters.

The length scale over which bed slope should be measured is difficult to estimate owing to the variability of bed roughness over several ice thicknesses in our study region[12,44]. Therefore, we chose to derive the bed slope from calculations before the onset of summer melting and the associated increase in velocity. During this window, we assume that vertical strain and the rate of cavity opening are constant, yielding:

$$\alpha = \tan^{-1}\left(\frac{w_{s,bg} - \dot{\varepsilon}_{zz,bg} H}{u_{b,bg}}\right) \quad (5)$$

where the subscript 'bg' represents background conditions.

We note that diurnal variations in bed separation are generally within the range of error. Our results suggest that vertical strain is a non-negligible contribution to vertical motion in regions of the GIS (Extended Data Fig. 2); simply removing the bed-parallel component of bed separation while assuming that $\dot{\varepsilon}_{zz}$ is negligible may result in inaccurate estimates of bed separation.

Melt events. During 2011 and 2012, an automatic weather station measured a wide range of atmospheric conditions every 5 min, including ablation, incoming and reflected short-wave radiation, wind speed and direction, humidity and the air temperature at a height of 2 m above the ice surface. To quantitatively constrain melt events, we simply difference consecutive calculations of 24-hour average temperature (with noon Coordinated Universal Time (UTC) as the midpoint). A positive temperature differential (that is, an increase in the 24-hour average temperature) of 0.5 °C is considered a melt event. To limit visual confusion, the start of the melt event is plotted as the minimum of the first day and the maximum of the last day of the melt event (Fig. 2).

Cross-correlation analysis. To characterize the lead–lag relationship between borehole hydraulic head, moulin hydraulic head and ice velocity, we performed cross-correlation analyses. We used the maximum cross-correlation coefficients and associated lags to examine the temporal relationship between various time series[17] (Extended Data Table 2).

The ice velocities used for cross-correlation analysis have a 1-hour moving average applied to reduce spurious noise[13] but still maintain independence between velocity measurements used in this analysis. We then decimated ice velocity and hydraulic head measurements to a 1-hour sampling interval. For moulins 3 and 4, we use a 5-min sampling interval to determine more closely a potential lagged relationship. We detrended all data using a 24-hour moving window mean and recorded measurements as standardized residuals[17]. Data gaps, which primarily occur in velocity data (~3% during both years), are filled using linear interpolation. Less than 1% (and generally 0%) of borehole and moulin data were linearly interpolated in either year; the exception being the FOXX moulin data, with 6% in 2011. All re-expressed time series, except the FOXX moulin, approximate a Gaussian distribution with a mean centred at zero. Because the FOXX moulin does not approximate a Gaussian distribution, we do not present cross-correlation analysis that includes the FOXX moulin.

Borehole hydraulic head and ice velocity exhibit the strongest inverse correlation with a lag of ~4 hours. As 1-hour averaged ice velocities have inherently higher errors than 6-hour averaged ice velocities, correlation coefficients with ice velocity are low but still significant (Extended Data Table 2). Moulins 3 and 4 are strongly correlated at zero lag (Extended Data Table 2), despite having differing supraglacial inputs and geometries, suggesting pressure equalization within the channelized subglacial system[23].

Subglacial channel geometry. Recent evidence suggests that characteristics of the GIS ablation zone distal from the margin (low surface slope and limited conduit meltback) prevent the formation of an extensive channelized system[6]. However, dye tracing suggests the presence of channelization through much of the ablation area[3]. Our moulin observations indicate a component of the subglacial system that is efficiently conducting the available melt water. However, this may be the result of an efficient distributed pathway[6]. To characterize the nature of the efficient system we performed a simple numerical analysis to explore the channel stability in our study area.

Using the hydraulic head of moulin 3 and supraglacial discharge estimated from ablation measurements at the FOXX weather station, we calculated the change in channel geometry over ~30 days in 2012, following previous work[6,15]:

$$\frac{dS}{dt} = c_1 Q \Psi + u_b h_b - c_2 N^n S \quad (6)$$

where subglacial discharge Q is calculated as a function of moulin head h_m and supraglacial input, Q_{sur}:

$$Q = Q_{sur} - \frac{dh_m}{dt} S_m \quad (7)$$

and Ψ is the hydraulic gradient calculated as a function of downstream (indicated by subscript 'j') hydraulic head:

$$h_j = h_m + z_j - z_m - \frac{l_{m,j} c_3}{\rho_w g} Q^2 S_{m,j}^{-5/2} \quad (8)$$

Effective pressure N was calculated at the point midway between h_m and h_j. Additional parameters are listed in Extended Data Table 3.

For these calculations, we set $u_b h_b = 0$ to clarify the role of creep closure and channel melt-back in the maintenance of subglacial channels. This assumption is applicable for our data set because we measure pressures after the assumed onset of channelization[4]. Once channels are larger than bedrock bumps, cavity opening due to sliding probably plays a very limited part in continued channelization[15]. Initial subglacial channel size is determined by initiating the model with a small channel and sinusoidal inputs approximating the daily average and range of moulin 3's head and supraglacial discharge into the modelled moulin until the channel size stabilizes. With this approach we cannot specifically address the timescale of channel development because we do not constrain supraglacial input and moulin hydraulic head at the beginning of the melt season. After determining the initial channel size, we forced the system with observations of supraglacial input and the hydraulic head of moulin 3 (Extended Data Fig. 4). Supraglacial input is calculated by scaling ablation measurements to half of the moulin 3 drainage basin area[45]. As moulin hydraulic head exceeds floatation only rarely, we assumed that all water entering the moulin enters and stays within the channelized system over the short distance assessed here. This assumption is conservative with respect to maximum channel melt back.

Using a distance (1.5 km) and a bed and surface slope similar to those of our study area, we were able to qualitatively reproduce the head difference between moulins 3 and 4 using this simple numerical analysis (Extended Data Fig. 4). Although this analysis cannot directly address the timescale of channel development, it does suggest that with the observed supraglacial input and moulin hydraulic head, subglacial channels can be maintained in our study area. However, we do note that supraglacial melt perturbations may be required to sustain channels over long periods; so steady-state modelling may be insufficient to explore the spatial extent of subglacial channels under the GIS. These calculations suggest that periods with elevated hydraulic gradients, probably during and shortly after melt events, allow for increased melting to effectively counter creep closure (Extended Data Fig. 4). This melting results in channel enlargement; however, during periods of normal diurnal variability, the available supraglacial melt and the associated hydraulic gradient are generally lower, resulting in rapid channel closure. Regular melt events may be essential in the maintenance of subglacial channels in this region of the GIS.

Recent studies indicate that increased efficiency of subglacial channels during high melt years could result in the observed decline in late season ice velocities through more extensive drainage of the bed following the cessation of surface melting[9,10]. However, our results suggest that the rapid adjustment of subglacial channels to the available melt, and the need for melt events to open the conduits periodically, may preclude this possibility. Instead, the observed declines in ice velocity[1,9,10,13], may be the result of changes in unchannelized regions of the subglacial system.

Potential mechanisms for borehole diurnal variability. Although the boreholes in this study connected to the bed, there are several lines of evidence that suggest borehole pressures are responding to pressure variations due to basal sliding rather than the direct propagation of water pressure pulses at the bed. First, during 2011 (and mostly during 2012), borehole hydraulic heads are always higher than those of the moulin that is only 300 m away, thus preventing the propagation of water from the channelized system to the borehole locations. Second, if pressure fluctuations in our boreholes resulted from propagation of diurnal pulses from channels to boreholes through till, we would expect boreholes further from the channel to exhibit smaller and more lagged peak diurnal water pressures. In contrast, we find that water-pressure maxima and minima in boreholes display no consistent pattern in lag times (Fig. 2), and cross-correlation analysis indicates that lag does not increase as a function of distance from the moulin in 2011 (Extended Data Table 2). Third, we computed the hydraulic diffusivity needed to produce the observed 15-h phase lag between moulin and borehole pressure peaks following ref. 18:

$$D = \frac{x^2}{2\omega t^2} \quad (9)$$

where x and t are the distance and time lag, respectively, between the channel and the borehole sensor and ω is the angular frequency of the periodic boundary condition ($\omega = 7.27 \times 10^{-5}\ s^{-1}$ for a diurnal cycle). This calculation results in a diffusivity of approximately $10^{-1}\ m^2\ s^{-1}$, several orders of magnitude larger than

expected hydraulic diffusivities for glacial till[46] and in the range of the hydraulic diffusivity for rock[47] and yet there is evidence of thick sediments beneath our field area[25]. Fourth, borehole minima are more closely correlated to moulin and velocity maxima (Extended Data Table 2). As a result, we do not believe that the pressure lag observed in the borehole record results from diffusion of the moulin-generated pressure wave through subglacial sediments. These observations and recent modelling results[7] lead us to conclude that borehole-pressure fluctuations result from non-locally forced ice motion. In this case, we expect and observe the pressure fluctuations in the boreholes to scale with diurnal velocity variability (Fig. 3).

Flow coupling and mechanical support transfer. To constrain the mechanism driving changing pressures measured via boreholes, we examine the relationship between the diurnal range in borehole hydraulic head and the diurnal ranges in both ice velocity and moulin hydraulic head. Borehole water levels are anti-correlated with horizontal ice velocity and moulin water level (Figs 2 and 3a, b). Such anti-correlated behaviour has been observed on alpine glaciers and is generally hypothesized to occur through the transfer of mechanical support between the efficient and weakly connected regions of the bed[17–19,22]. In our study, the two components are represented by the moulin and borehole water levels, respectively. However, if load transfer is the only mechanism controlling borehole water pressure, diurnal changes in borehole water level should be most strongly anti-correlated with diurnal changes in moulin water level. Instead, the diurnal magnitude of borehole head is more strongly anti-correlated with the diurnal magnitude of ice velocity, as follows. For moulin 3, (~day 192–240), borehole 4 $r^2 = 0.68$ ($p < 0.05$; $n = 89$), borehole 6 $r^2 = 0.70$ ($p < 0.05$; $n = 88$), borehole 7 $r^2 = 0.72$ ($p < 0.05$; $n = 85$). For ice velocity, (~day 192–240), borehole 4 $r^2 = 0.75$ ($p < 0.05$; $n = 80$), borehole 6 $r^2 = 0.80$ ($p < 0.05$; $n = 79$), borehole 7 $r^2 = 0.81$ ($p < 0.05$; $n = 75$)). Local load transfer would also result in moulin water levels and borehole pressures to be directly out of phase[22]. We observe that minimum daily borehole pressures consistently lag daily maximum ice velocity and moulin water level by about 4 hours (Extended Data Table 2), further suggesting that flow coupling may be important in controlling unchannelized regions of the bed[21].

Moulin–velocity hysteresis. To examine the relationship between moulin hydraulic head and ice velocity over the course of the observation period, we plot moulin hydraulic head against ice velocity. During 2011 and 2012, the relationship between moulin hydraulic head and ice velocity changes, showing a decreasing trend in velocity without a similar change in moulin hydraulic head. Diurnal hysteresis is evident in both years (Extended Data Fig. 4).

GULL borehole observations. During the 2011 field season, a series of boreholes were also drilled and instrumented at GULL (69° 27′ N, 49° 43′ W), a site approximately 5 km up the flow line from FOXX. These boreholes were less than 500 m downstream of a moulin slowly draining a supraglacial lake. As at FOXX, pressure transducers were installed in three boreholes; however, owing to a highly deformable layer of ice, sensor cables sheared before the start of the 2012 melt season[7]. Borehole head at GULL demonstrates small diurnal variations that are out of phase with velocity. Yet, despite a temporally limited water pressure record, we observe similar trends in decreasing daily minimum velocity and borehole head values and borehole head as observed at FOXX during the 2012 melt season (Extended Data Fig. 5). Although these are observations are limited by the borehole spatial distribution, this trend suggests that these long-term dynamic changes may be widespread.

31. Iken, A., Echelmeyer, K. & Harrison, W. D. in *Ice Core Drilling* (eds Rado, C. & Beaudoing, D.) *Proc. Third Int. Workshop on Ice Drilling Technology (Grenoble, 10–14 October)* 123–134 (Laboratoire de Glaciology et Géophysique de l'Environment, 1988).
32. Humphrey, N. & Echelmeyer, K. Hot-water drilling and bore-hole closure in cold ice. *J. Glaciol.* **36,** 287–298 (1990).
33. Holmlund, P. & Hooke, R. LeB. High water-pressure events in moulins, Storglaciären, Sweden. *Geogr. Ann. A* **65,** 19–25 (1983).
34. Iken, A. Measurements of water pressure in moulins as part of a movement study of the White Glacier, Axel Heiberg Island, Northwest Territories, Canada. *J. Glaciol.* **11,** 53–58 (1972).
35. Vieli, A., Jania, J., Blatter, H. & Funk, M. Short-term velocity variations on Hansbreen, a tidewater glacier in Spitsbergen. *J. Glaciol.* **50,** 389–398 (2004).
36. Werder, M. A., Loye, A. & Funk, M. Dye tracing a jökulhlaup: I. Subglacial water transit speed and water-storage mechanism. *J. Glaciol.* **55,** 889–898 (2009).
37. Chen, G. *GPS Kinematic Positioning for Airborne Laser Altimetry at Long Valley, California.* PhD thesis, MIT (1998); http://dspace.mit.edu/handle/1721.1/9680.
38. Mair, D., Nienow, P., Sharp, M., Wohlleben, T. & Willis, I. Influence of subglacial drainage system evolution on glacier surface motion: Haut Glacier d'Arolla, Switzerland. *J. Geophys. Res.* **107,** http://dx.doi.org/10.1029/2001JB000514 (2002).
39. Mair, D., Sharp, M. J. & Willis, I. C. Evidence for basal cavity opening from analysis of surface uplift during a high-velocity event: Haut Glacier d'Arolla, Switzerland. *J. Glaciol.* **48,** 208–216 (2002).
40. Anderson, R. L. *et al.* Strong feedbacks between hydrology and sliding of a small alpine glacier. *J. Geophys. Res.* **109,** F03005 (2004).
41. Sugiyama, S. & Gudmundsson, H. Short-term variations in glacier flow controlled by subglacial water pressure at Lauteraargletscher, Bernese Alps, Switzerland. *J. Glaciol.* **50,** 353–362 (2004).
42. Harper, J. T., Humphrey, N. F., Pfeffer, W. T. & Lazar, B. Two modes of accelerated glacier sliding related to water. *Geophys. Res. Lett.* **34,** L12503 (2007).
43. Howat, I. M., Tulaczyk, S., Waddington, E. & Björnsson, H. Dynamic controls on glacier basal motion inferred from surface ice motion. *J. Geophys. Res.* **113,** F03015 (2008).
44. Catania, G. A., Neumann, T. A. & Price, S. F. Characterizing englacial drainage in the ablation zone of the Greenland Ice Sheet. *J. Glaciol.* **54,** 567–578 (2008).
45. McGrath, D., Colgan, W., Steffen, K., Lauffenburger, P. & Balog, J. Assessing the summer water budget of a moulin basin in the Sermeq Avannarleq ablation region, Greenland ice sheet. *J. Glaciol.* **57,** 954–964 (2011).
46. Paterson, W. S. B. *The Physics of Glaciers* 3rd edn, 60 (Pergamon, 1994).
47. Li, V. Estimation of in-situ hydraulic diffusivity of rock masses. *Pure Appl. Geophys.* **122,** 545–559 (1985).

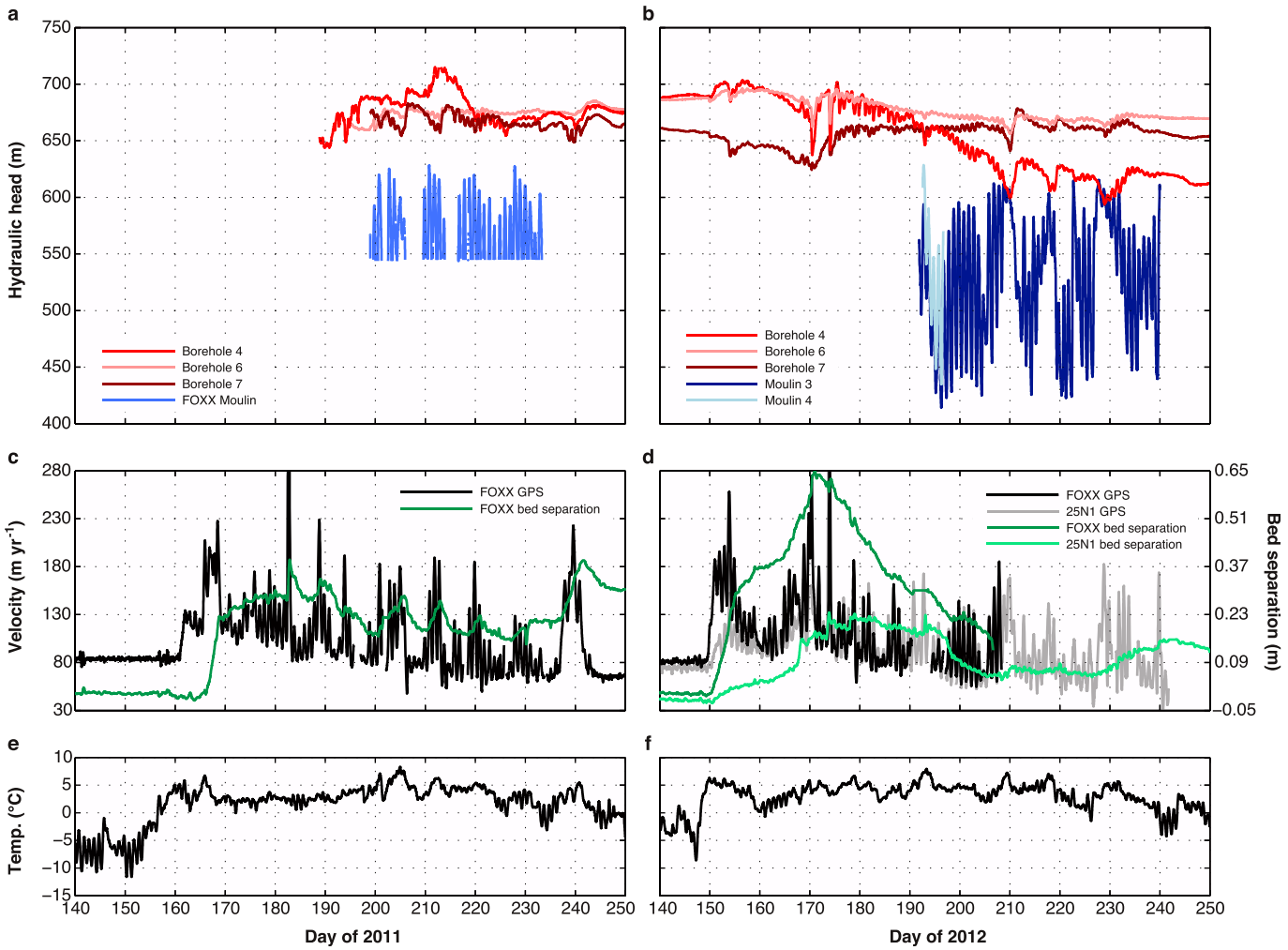

Extended Data Figure 1 | Borehole and moulin head and ice-surface velocity over two melt seasons. **a**, 2011 measurements from FOXX moulin (blue), borehole 7 (dark red), borehole 6 (pink) and borehole 4 (red). **b**, 2012 measurements from moulin 3 (navy) and moulin 4 (light blue). **c**, 2011 ice velocity (black) and bed separation (green) for FOXX. Peak velocity on day 182 is 402.3 m yr^{-1} (exceeding the *y*-axis limit). **d**, 2012 ice velocity and bed separation for FOXX and 25N1 (grey, light green). Peak velocity for FOXX and 25N1 (312 m yr^{-1} and 337 m yr^{-1}) occurred on day 173. **e**, **f**, 6-h averaged air temperature for 2011 and 2012. Grey bars are melt events.

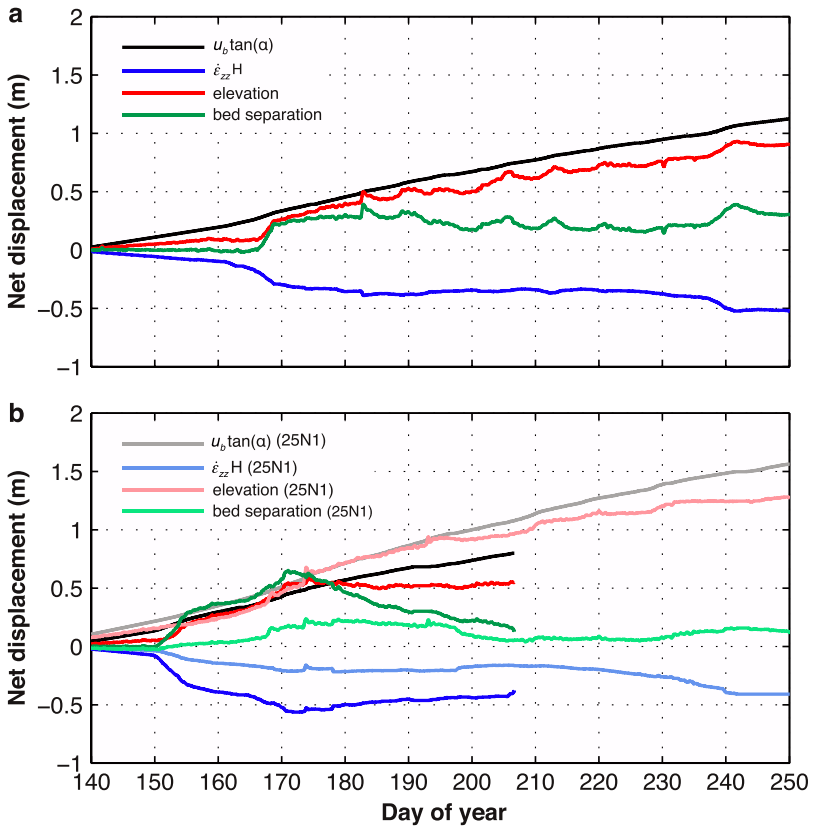

Extended Data Figure 2 | Components of vertical motion 2011 and 2012. **a**, Components of vertical motion for 2011 at FOXX. Bed parallel motion (u_b tan(α); black), strain thickening and thinning ($\dot{\varepsilon}_{zz}H$; blue), elevation with measured winter elevation removed (red), and calculated bed separation (green). **b**, Components of vertical motion for 2012. Colours as in **a** for FOXX. Lighter colours correspond to components of vertical motion from 25N1.

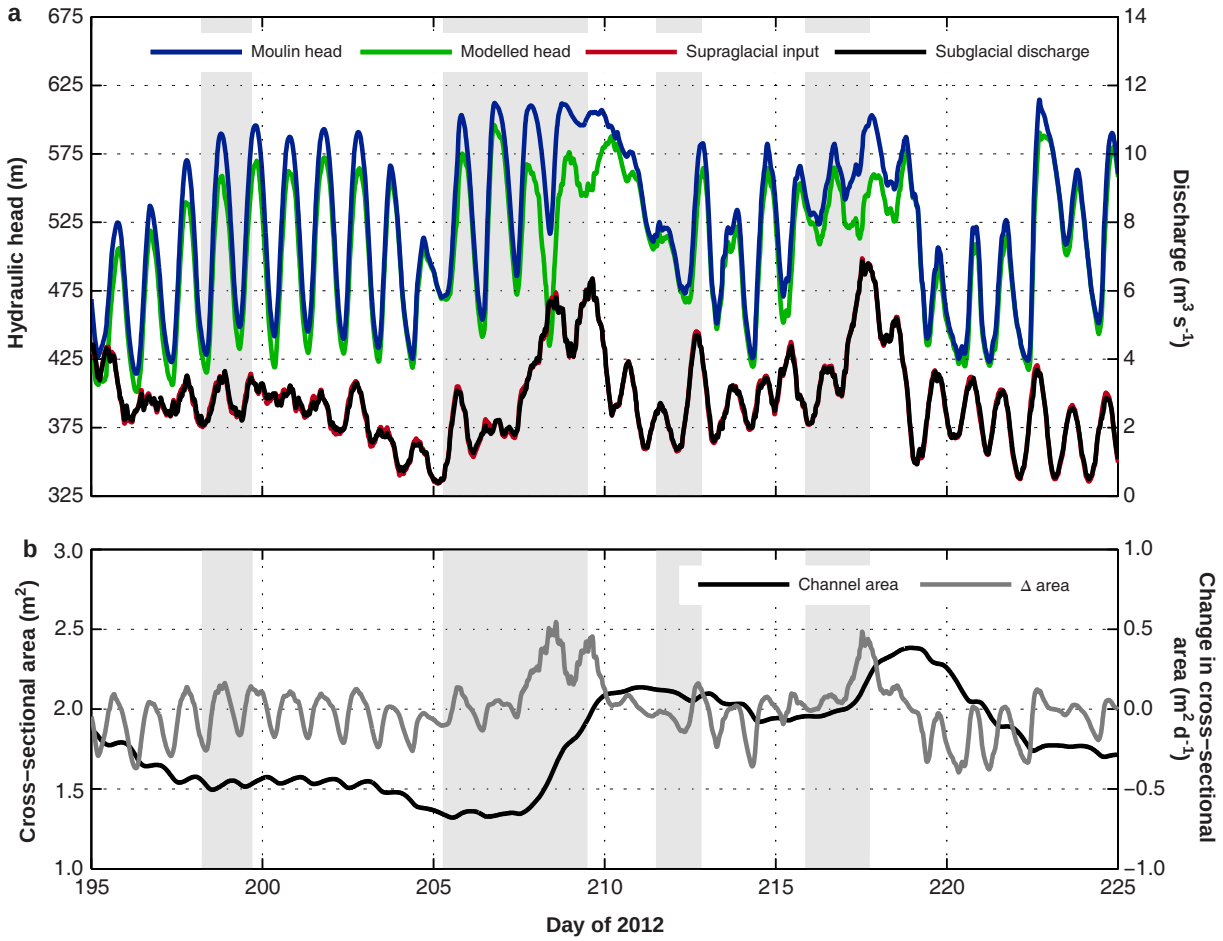

Extended Data Figure 3 | Modelled hydraulic head and conduit geometry. **a**, Moulin 3 head (blue) and supraglacial input (red) are model inputs. Predicted downstream head is calculated from equation (8) (green). Subglacial discharge (black) is calculated as a function of head change and supraglacial inputs. It does not vary significantly from supraglacial input even when a large (~20 m^2) moulin geometry is used. **b**, Modelled subglacial channel cross-sectional area (black) changes rapidly (grey) during and shortly after expected melt events (grey bars).

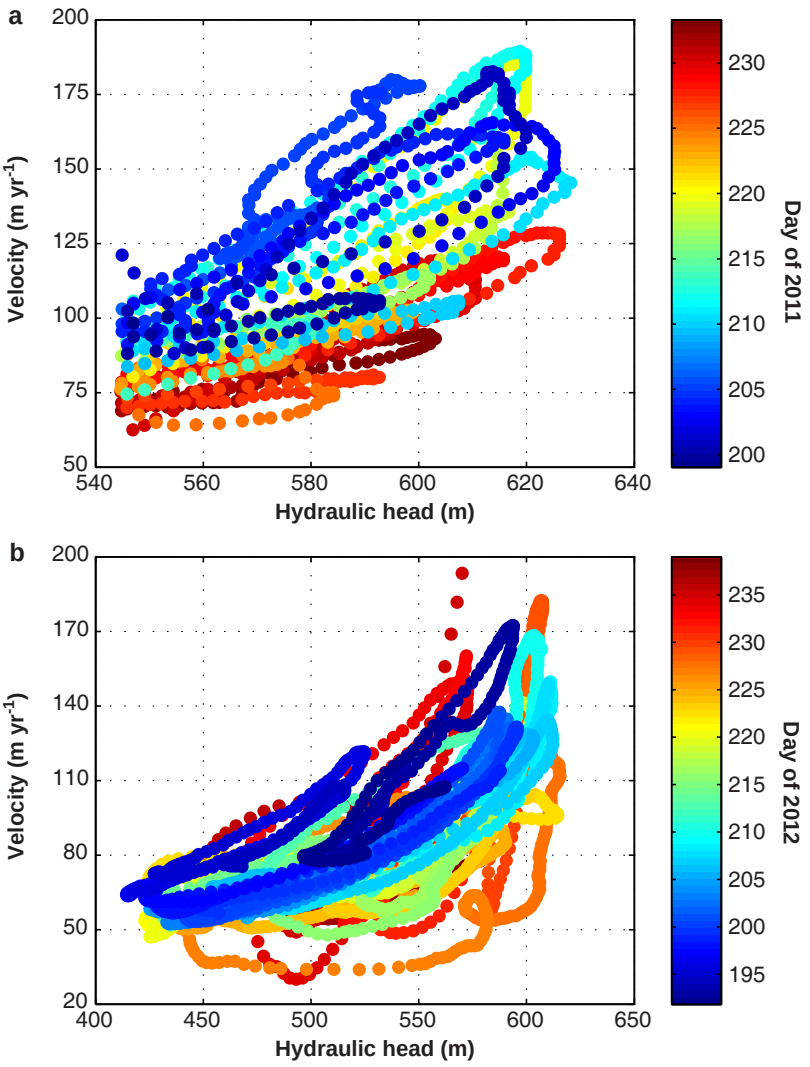

Extended Data Figure 4 | Seasonal relationship between moulin head and ice velocity for 2012 and 2011. Moulin hydraulic head and associated ice velocity data plotted every 15 min over the course of the measurement periods for 2011 (**a**) and 2012 (**b**). 2011 data are truncated below 543 m by the high elevation of the moulin sensor.

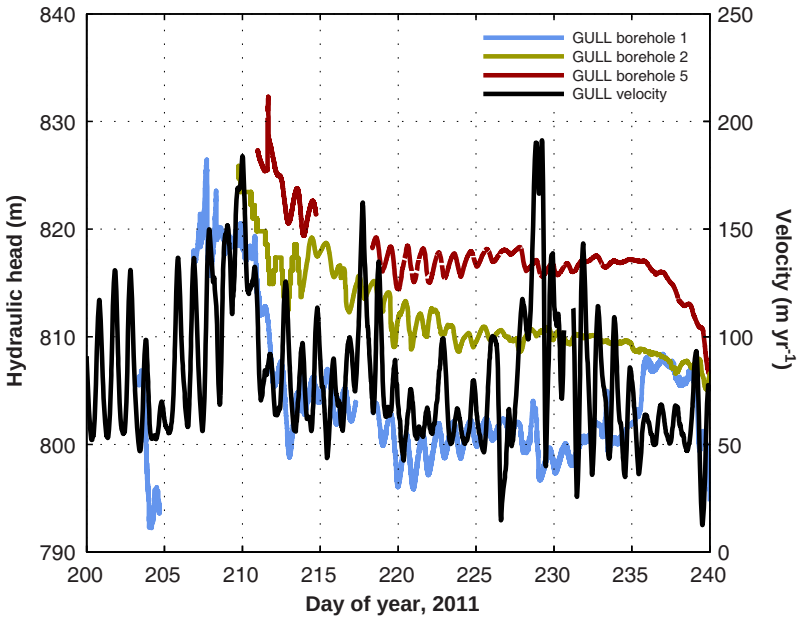

Extended Data Figure 5 | Borehole hydraulic heads and ice velocity at GULL during 2011. Three hydraulic head records (red, yellow, blue) from boreholes located ~0.5 km from a moulin. Ice velocity from GULL GPS (black), ~0.75 km south of GULL boreholes.

Extended Data Table 1 | Site coordinates and characteristics

Field site	Latitude	Longitude	Elevation (m)	Ice thickness (m)	Surface characteristics
FOXX GPS & weather station	69.4458	-49.8847	706	602*	uncrevassed, in small basin
25N1 GPS	69.4454	-49.7890	851	608*	local crevasses
Borehole 4	69.4456	-49.8802	706	624	uncrevassed, near large supraglacial stream
Borehole 6	69.4463	-49.8807	706	614	uncrevassed, near large supraglacial stream
Borehole 7	69.4464	-49.8805	706	623	uncrevassed, near large supraglacial stream
FOXX moulin	69.4446	-49.8859	703	620*	supraglacial stream entering from the northeast
Moulin 3	69.4358	-49.9092	657	564*	supraglacial streams entering from the east & west
Moulin 4	69.4296	-49.8785	709	540*	supraglacial stream entering from the east

Location and surface elevations determined from GPS. Ice thicknesses at borehole locations determined during drilling. *Ice thicknesses interpolated from CReSIS radar sounding data[30].

Extended Data Table 2 | Cross-correlation analysis

	2011		2012			
	Observation period (day 195 to 235)		Melt season (day 150 to 240)		Moulin period (day 192 to 240)	
	Peak to minimum	Peak to peak	Peak to minimum	Peak to peak	Peak to minimum	Peak to peak
Borehole 4/ ice velocity	-0.15 (7)	0.16 (18)	-0.45 (5)	0.38 (16)	-0.49 (4)	0.46 (16)
Borehole 6/ ice velocity	-0.21 (1)	0.23 (17)	-0.38 (5)	0.34 (16)	-0.49 (3)	0.46 (15)
Borehole 7/ ice velocity	-0.39 (4)	0.39 (15)	-0.42 (5)	0.39 (16)	-0.44 (4)	0.43 (16)
Moulin 3/ ice velocity	--	--	--	--	0.48 (0)	-0.45 (-13)
Borehole 4/ moulin 3	--	--	--	--	-0.83 (4)	0.75 (16)
Borehole 6/ moulin 3	--	--	--	--	-0.80 (2)	0.74 (14)
Borehole 7/ moulin 3	--	--	--	--	-0.76 (3)	0.69 (16)
Moulin 4/ moulin 3	--	--	--	--	1.00 (0)	-0.80 (11.5)

Maximum positive and negative correlation coefficient between indicated data sets; lag times are noted in parentheses. In 2011, sample sizes for borehole 4, borehole 6 and borehole 7 cross-correlations are $n = 1{,}105$, 981 and 839, respectively. For the 2012 melt season, $n = 2{,}159$. Between days 192 and 240 of 2012, $n = 1{,}155$. The moulin 4 to moulin 3 cross-correlation sample size is $n = 901$. The 99% confidence interval for all cross-correlation coefficients is less than 0 ± 0.1. Negative lags indicate that the first series leads the second series.

Extended Data Table 3 | Parameters used in conduit-geometry calculations

Symbol	Value	Parameter
A	5.3e-24 Pa^{-3} s^{-1}	Glen's flow law coefficient
c_t	7.5e-8 J kg^{-1} K^{-1}	Pressure melting coefficient
c_w	4.22e3 J kg^{-1} K^{-1}	Specific heat capacity, ice
f	0.1	Friction factor
n	3	Glen's flow law exponent
L	3.35e5 J kg^{-1}	Latent heat of fusion
ρ_i	910 kg m^{-3}	Density of ice
ρ_w	1,000 kg m^{-3}	Density of water
h_b	m	Bedrock bump height
S	m^2	Conduit cross-sectional area
S_m	m^2	Moulin cross-sectional area
u_b	m a^{-1}	Basal sliding velocity
z	m	Bed elevation
Ψ	Pa m^{-1}	Hydraulic gradient
N	$\rho_i g h_i - \rho_w g h_w$	Effective pressure
c_1	$(1 - \rho_w c_t c_w)/\rho_i L$	Melting parameter
c_2	$2An^{-n}$	Closing parameter
c_3	$(\pi + 2)\rho_w f / 2^{5/2}\pi^{1/2}$	